The Magnetorotational Instability in a Collisionless Plasma

Eliot Quataert,[1] William Dorland,[2,3] and Greg Hammett[2,4]

ABSTRACT

We consider the linear axisymmetric stability of a differentially rotating collisionless plasma in the presence of a weak magnetic field; we restrict our analysis to wavelengths much larger than the proton Larmor radius. This is the kinetic version of the magnetorotational instability explored extensively as mechanism for magnetic field amplification and angular momentum transport in accretion disks. The kinetic calculation is appropriate for hot accretion flows onto compact objects and for the growth of very weak magnetic fields, where the collisional mean free path is larger than the wavelength of the unstable modes. We show that the kinetic instability criterion is the same as in MHD, namely that the angular velocity decrease outwards. However, nearly every mode has a linear kinetic growth rate that differs from its MHD counterpart. The kinetic growth rates also depend explicitly on β, i.e., on the ratio of the gas pressure to the pressure of the seed magnetic field. For $\beta \sim 1$ the kinetic growth rates are similar to the MHD growth rates while for $\beta \gg 1$ they differ significantly. For $\beta \gg 1$, the fastest growing mode has a growth rate $\approx \sqrt{3}\Omega$ for a Keplerian disk, larger than its MHD counterpart; there are also many modes whose growth rates are negligible, $\lesssim \beta^{-1/2}\Omega \ll \Omega$. We provide a detailed physical interpretation of these results and show that gas pressure forces, rather than just magnetic forces, are central to the behavior of the magnetorotational instability in a collisionless plasma. We also discuss the astrophysical implications of our analysis.

Subject Headings: accretion, accretion disks; instabilities; plasmas

---

[1]UC Berkeley, Astronomy Department, 601 Campbell Hall, Berkeley, CA 94720; eliot@astron.berkeley.edu

[2]Imperial College, Blackett Laboratory, Prince Consort Rd, London SW7 2BW, UK

[3]bdorland@kendall.umd.edu

[4]Permanent Address: Princeton Plasma Physics Laboratory, P. O. Box 451, Princeton, NJ, 08543; hammett@princeton.edu

1. Introduction

Balbus & Hawley (1991; BH91) showed that differentially rotating accretion disks are linearly unstable in the presence of a weak magnetic field (see Balbus & Hawley 1998 for a review; BH98). This instability, known as the "magnetorotational instability" (MRI), is local and extremely powerful, with a growth rate comparable to the rotation frequency of the disk. MHD turbulence resulting from the MRI is the most promising source of the efficient angular momentum transport needed in astrophysical accretion flows (e.g., Hawley, Gammie, & Balbus 1995; Armitage 1998; Hawley 2000; Stone & Pringle 2001). The MRI may also be important for the dynamo generation of galactic and stellar magnetic fields.

In this paper we present a linear analysis of the MRI in a collisionless plasma using kinetic theory. The kinetic calculation is appropriate whenever the wavelength of the unstable modes is shorter than the collisional mean free path. This regime is astrophysically interesting for several reasons:

(1) In MHD, the most unstable mode of the MRI has a wavelength $\lambda \approx v_A/\Omega$, where $v_A = B/\sqrt{4\pi\rho}$ is the Alfvén speed and Ω is the rotation frequency of the disk. Thus, for a very weak magnetic field, the fastest growing mode has a very short wavelength, less than the collisional mean free path in many cases. A kinetic treatment is therefore required to determine whether the MRI can amplify very weak fields (e.g., the "first" magnetic fields generated at high redshift by a Biermann battery or analogous mechanism).

(2) Radiatively inefficient accretion flows onto compact objects provide a useful framework for interpreting observations of low-luminosity X-ray binaries and active galactic nuclei (see, e.g., Ichimaru 1977; Rees et al. 1982 [the ion torus model]; Narayan & Yi 1995 [ADAFs]; for a review see Narayan et al. 1998 or Quataert 2001). In such models, the accreting gas is a hot two-temperature plasma in which the proton temperature ($\sim 10^{12}$ K near a black hole) is much larger than the electron temperature ($\sim 10^9 - 10^{11}$ K). In order to maintain such a two-temperature configuration, the accretion flow must be effectively collisionless in the sense that the timescale for electrons and protons to exchange energy by Coulomb collisions is longer than the inflow time of gas in the accretion disk. In principle, a kinetic treatment of the accretion flow structure, rather than a fluid treatment, is therefore necessary. The calculations described in this paper represent a first step towards understanding the physics of angular momentum transport and the structure of the accretion flow using kinetic theory.

Our analysis is restricted to wavelengths much larger than the proton Larmor radius and frequencies below the proton cyclotron frequency. To motivate why kinetic effects can be important even on these "large" scales, consider a uniform medium threaded by a weak magnetic field ($\beta \gg 1$, where β is the ratio of the gas pressure to the magnetic pressure).

There are three long-wavelength waves in such a system: (1) the sound wave, (2) the Alfvén wave, and (3) the slow magnetosonic wave. It is well known that the sound wave and the slow wave are very different in a collisionless plasma than in collisional plasmas described by MHD (e.g., Barnes 1966). We shall see that the same is true for the MRI.

This paper is organized as follows. In the next section we describe our basic equations and assumptions (§2). In §3 we discuss linear waves in a collisionless plasma, emphasizing an important difference between MHD and kinetic theory that is useful for understanding the kinetic MRI results. In §4 we numerically solve the kinetic MRI dispersion relation and discuss its physical interpretation. We also show that a generalization of Balbus & Hawley's (1992; BH92) "spring" model of the MRI captures the main results of the kinetic calculation. Finally, in §5 we summarize our results and discuss their astrophysical implications.

2. Basic Equations

In the limit that all fluctuations of interest have wavelengths much larger than the proton Larmor radius and frequencies much less than the proton cyclotron frequency, a collisionless plasma can be described by the following fluid equations (e.g., Kulsrud 1983; Snyder, Hammett, & Dorland 1997):

$$\frac{\partial \rho}{\partial t} + \nabla \cdot (\rho \mathbf{V}) = 0, \tag{1}$$

$$\rho \frac{\partial \mathbf{V}}{\partial t} + \rho (\mathbf{V} \cdot \nabla) \mathbf{V} = \frac{(\nabla \times \mathbf{B}) \times \mathbf{B}}{4\pi} - \nabla \cdot \mathbf{P} + \mathbf{F_g}, \tag{2}$$

$$\frac{\partial \mathbf{B}}{\partial t} = \nabla \times (\mathbf{V} \times \mathbf{B}), \tag{3}$$

and

$$\mathbf{P} = p_\perp \mathbf{I} + (p_{||} - p_\perp) \hat{\mathbf{b}}\hat{\mathbf{b}}, \tag{4}$$

where ρ is the mass density, $\mathbf{V}$ is the fluid velocity, $\mathbf{B}$ is the magnetic field vector, $\mathbf{F_g}$ is the force due to gravity, $\mathbf{b} = \mathbf{B}/|\mathbf{B}|$ is a unit vector in the direction of the magnetic field, and $\mathbf{I}$ is the unit tensor. Equations (1)-(3) are identical to the basic equations of (collisional) MHD except that the pressure, $\mathbf{P}$, is a tensor that is generally different perpendicular ($p_\perp$) and parallel ($p_{||}$) to the background magnetic field (e.g., the temperature need not be isotropic in a collisionless plasma). Formally, the pressure in equation (4) should contain a sum over all particle species in the plasma (electrons, protons, and ions). In what follows, however, we consider a single fluid model in which only one contribution to the pressure response is included. In practice, the ions dominate the dynamics under consideration and so the pressure can be interpreted as the ion pressure. This is particular true for hot accretion flows in which $T_p \gg T_e$.

In a collisionless plasma, the parallel and perpendicular pressures satisfy separate "equations of state" given by (e.g., Chew, Goldberger, & Low 1956):

$$\rho B \frac{d}{dt}\left(\frac{p_\perp}{\rho B}\right) = -\nabla\cdot(\hat{\mathbf{b}} q_\perp) - q_\perp \nabla\cdot\hat{\mathbf{b}} \tag{5}$$

and

$$\frac{\rho^3}{B^2}\frac{d}{dt}\left(\frac{p_{||}B^2}{\rho^3}\right) = -\nabla\cdot(\hat{\mathbf{b}} q_{||}) - 2q_\perp \nabla\cdot\hat{\mathbf{b}}, \tag{6}$$

where $d/dt = \partial/\partial t + \mathbf{V}\cdot\nabla$ is the Lagrangian derivative, and $q_\perp$ and $q_{||}$ represent the flow of heat due to the motion of particles along magnetic field lines. Note that although there is no heat flow perpendicular to the magnetic field due to the very small proton Larmor radius, the perpendicular pressure/temperature can change due to heat transport along the magnetic field and so $q_\perp \neq 0$. If one neglects the heat flux terms, equations (5) and (6) reduce to "double adiabatic theory" (Chew et al. 1956). Equation (5) then describes the invariance of the average magnetic moment of the plasma, $\mu \propto T_\perp/B \propto p_\perp/(\rho B)$, where $T_\perp$ is the perpendicular temperature. And equation (6) describes adiabatic parallel pressure changes due to the expansion or contraction of fluid elements (Kulsrud 1983).

Equations (1)-(6) can be rigorously derived by expanding the Vlasov equation in the long wavelength, low frequency limit, and taking velocity moments (e.g., Kulsrud 1983). They face, however, the usual problem that the heat fluxes $q_\perp$ and $q_{||}$ depend on the third moments of the particle distribution function and so additional equations are needed to "close" the moment hierarchy. In Kulsrud's kinetic MHD one avoids this closure problem by solving the drift-kinetic equation, which is the low-frequency, long-wavelength, limit of the Vlasov equation (see Kulsrud 1983). By taking moments of the resulting distribution function one calculates $p_\perp$ and $p_{||}$ for use in equation (2). For linear problems this approach is not too difficult and is the one employed here (see eqs. [14] and [15] below). For nonlinear problems, however, it is much more involved. Snyder et al. (1997) developed fluid approximations for $q_\perp$ and $q_{||}$ that model kinetic effects such as Landau damping and phase mixing. In this approach one solves equations (5) and (6) instead of solving for the full distribution function. For nonlinear problems, this is computationally more efficient and is a possible way of using MHD codes to extend the linear results of this paper to the nonlinear regime.[5]

---

[5]Although we use the full drift-kinetic equation to calculate $p_\perp$ and $p_{||}$, we have also found that the closures in Snyder et al. (1997) provide an excellent approximation for the linear problems considered here.

2.1. Linear Perturbations

We assume that the background (unperturbed) plasma is described by a non-relativistic Maxwellian distribution function with equal parallel and perpendicular pressures (temperatures). Although the equilibrium pressure is assumed to be isotropic, the perturbed pressure will not be, which is a crucial difference between the kinetic and MHD problems. We take the plasma to be differentially rotating, but otherwise uniform (e.g., we neglect temperature and density gradients). Thus the velocity is given by $\mathbf{V} = \mathbf{V_0} + \delta\mathbf{v}$ where $\mathbf{V_0} = R\Omega\hat{\phi}$ and $\Omega(R)$ is the rotation rate. We consider a weak (subthermal) magnetic field with vertical ($B_z = B_0 \sin\theta$) and azimuthal ($B_\phi = B_0\cos\theta$) components, where $\theta = \tan^{-1}[B_z/B_\phi]$ is the angle between the magnetic field vector and the ϕ direction and B_0 is the magnitude of the seed field. In a differentially rotating plasma, a finite B_R leads to a time-dependent B_ϕ, which greatly complicates the kinetic analysis (unlike in MHD, where a time-dependent B_ϕ can be accounted for; e.g., BH91); we therefore set $B_R = 0$. Finally, we consider fluctuations of the form $\exp[-i\omega t + i\mathbf{k}\cdot\mathbf{x}]$, with $\mathbf{k} = k_R\hat{R} + k_z\hat{z}$, i.e., axisymmetric modes; we also restrict our analysis to local perturbations for which $|\mathbf{k}|R \gg 1$. Writing $\rho = \rho_0 + \delta\rho$, $\mathbf{B} = \mathbf{B_0} + \delta\mathbf{B}$, $p_\perp = p_0 + \delta p_\perp$, and $p_{||} = p_0 + \delta p_{||}$, and working in cylindrical coordinates, the linearized versions of equations (1)-(3) become:

$$\omega\delta\rho = \rho_0 \mathbf{k}\cdot\delta\mathbf{v} \tag{7}$$

$$-i\omega\rho_0\delta v_R - \rho_0 2\Omega\delta v_\phi = \frac{-ik_R}{4\pi}\left(B_z\delta B_z + B_\phi\delta B_\phi\right) + \frac{ik_zB_z\delta B_r}{4\pi} - ik_R\delta p_\perp \tag{8}$$

$$-i\omega\rho_0\delta v_\phi + \rho_0\delta v_R\frac{\kappa^2}{2\Omega} = \frac{ik_zB_z\delta B_\phi}{4\pi} - ik_z\sin\theta\cos\theta\left[\delta p_{||} - \delta p_\perp\right] \tag{9}$$

$$-i\omega\rho_0\delta v_z = \frac{-ik_zB_\phi\delta B_\phi}{4\pi} - ik_z\left[\sin^2\theta\delta p_{||} + \cos^2\theta\delta p_\perp\right] \tag{10}$$

$$\omega\delta B_r = -k_zB_z\delta v_R \tag{11}$$

$$\omega\delta B_\phi = -k_zB_z\delta v_\phi - \frac{ik_zB_z}{\omega}\frac{d\Omega}{d\ln R}\delta v_R + B_\phi\mathbf{k}\cdot\delta\mathbf{v} \tag{12}$$

$$\omega\delta B_z = k_RB_z\delta v_R, \tag{13}$$

where $\kappa^2 = 4\Omega^2 + d\Omega^2/d\ln R$ is the epicyclic frequency. Equations (7)-(13) are very similar to the analogous equations in BH91 except that we do not impose incompressibility and the pressure response is anisotropic. In particular, note that, even though we consider axisymmetric modes, there is a pressure force in the ϕ-momentum equation (eq. [9]) because the perturbed pressure is anisotropic (i.e., $\hat{\phi}\cdot(\nabla\cdot\mathbf{P}) = ik_zP^{z\phi} = ik_z(\delta p_{||} - \delta p_\perp)\sin\theta\cos\theta$).

To complete our system of equations we need expressions for $\delta p_\perp$ and $\delta p_{||}$. These can be obtained by taking the second moments of the linearized and Fourier transformed drift-kinetic equation and are given by (e.g., eqs. 23-25 of Snyder et al. 1997)

$$\frac{\delta p_\perp}{p_0} = \frac{\delta \rho}{\rho_0} + D_1 \left(\frac{\delta B}{B_0}\right) \tag{14}$$

and

$$\frac{\delta p_{||}}{p_0} = \frac{\delta \rho}{\rho_0} + D_2 \left(\frac{\delta \rho}{\rho_0} - \frac{\delta B}{B_0}\right), \tag{15}$$

where $|\mathbf{B}| = B_0 + \delta B$, $\delta B = \hat{\mathbf{b}}_\mathbf{0} \cdot \delta \mathbf{B}$ is the parallel magnetic field perturbation, and

$$D_1 = 1 - R(\xi), \qquad D_2 = \left[\frac{1 + 2\xi^2 R(\xi) - R(\xi)}{R(\xi)}\right]. \tag{16}$$

Note that the second terms on the right hand side of equations (14) and (15) are the perpendicular and parallel temperature perturbations. In equation (16), $R(\xi) = 1 + \xi Z(\xi)$ is the plasma response function,

$$Z(\xi) = \frac{1}{\sqrt{\pi}} \int dx \frac{\exp[-x^2]}{x - \xi} \tag{17}$$

is the plasma dispersion function (e.g., Stix 1992), and $\xi = \omega/(\sqrt{2} c_0 |k_{||}|)$, where $k_{||} = \hat{\mathbf{b}} \cdot \mathbf{k}$ is the wavevector along the magnetic field and $c_0 = \sqrt{T/m}$ is the isothermal sound speed of the particles (we have absorbed Boltzmann's constant into T so as to not cause confusion with the wavevector).

Because equations (14) and (15) are rather different from the MHD equation of state it is worthwhile discussing their physical interpretation. Consider first fluctuations for which $\xi \gg 1$, in which case $Z(\xi) \approx -\xi^{-1} - 0.5\xi^{-3} - 0.75\xi^{-5}$, $R(\xi) \approx -0.5\xi^{-2} - 0.75\xi^{-4}$, $D_1 \approx 1$, and $D_2 \approx 2$. Equation (14) thus reduces to

$$\frac{\delta p_\perp}{p_0} \approx \frac{\delta \rho}{\rho_0} + \frac{\delta B}{B_0} \tag{18}$$

and equation (15) reduces to

$$\frac{\delta p_{||}}{p_0} \approx 3\frac{\delta \rho}{\rho_0} - 2\frac{\delta B}{B_0}. \tag{19}$$

These are the linearized double adiabatic equations (eqs. [5] and [6] with $q_\perp = q_{||} = 0$). Not surprisingly, the adiabatic limit requires $\omega \gg k_{||} c_0$, i.e., that the fluctuation timescale is much less than the time it takes particles to stream across the wavelength of the mode.

In the opposite limit, $\xi \ll 1$, $Z(\xi) \approx i\sqrt{\pi} - 2\xi$ and $R(\xi) \approx 1 + i\sqrt{\pi}\xi - 2\xi^2$, so that $D_1 \approx D_2 \approx -i\sqrt{\pi}\xi$. Equations (14) and (15) thus reduce to

$$\frac{\delta p_\perp}{p_0} \approx \frac{\delta \rho}{\rho_0} - i\sqrt{\pi}\xi \left(\frac{\delta B}{B_0}\right) \tag{20}$$

and

$$\frac{\delta p_{\|}}{p_0} \approx \frac{\delta \rho}{\rho_0} - i\sqrt{\pi}\xi\left(\frac{\delta \rho}{\rho_0} - \frac{\delta B}{B_0}\right). \tag{21}$$

These correspond to nearly isothermal fluctuations: the temperature perturbation is smaller than its "natural" value by a factor $\sim \xi \ll 1$. This is because $\omega \ll k_{\|} c_0$, i.e., particles stream across a wavelength on a timescale much less than the fluctuation timescale and efficiently wipe out temperature gradients. Equations (20) and (21) are the appropriate limit for the MRI. This is because the MRI has $|\omega| \lesssim k_z v_A$ and $\beta \gtrsim 1$, and so $\xi \lesssim \beta^{-1/2} \lesssim 1$.

2.2. The Dispersion Relation

To obtain the dispersion relation, we eliminate all non-velocity variables from the momentum equations. We first calculate $\delta B = \cos\theta \delta B_\phi + \sin\theta \delta B_z$ using δB_ϕ from equation (12) and δB_z from equation (13):

$$\frac{\delta B}{B_0} = \cos^2\theta \frac{\mathbf{k}\cdot\delta\mathbf{v}}{\omega} - \sin\theta\cos\theta\frac{k_z \delta v_\phi}{\omega} - i\frac{d\Omega}{d\ln R}\sin\theta\cos\theta\frac{k_z\delta v_R}{\omega^2} + \sin^2\theta\frac{k_R\delta v_R}{\omega}. \tag{22}$$

Substituting equations (7) and (22) into equations (14) and (15) then yields $\delta p_\perp$ and $\delta p_{\|}$ as functions of $\delta\mathbf{v}$, which we substitute into the perturbed momentum equations (eqs. [8]-[10]). Using the perturbed induction equations (eqs. [11]-[13]) we can also eliminate $\delta\mathbf{B}$ from the momentum equations in favor of $\delta\mathbf{v}$. This yields the following versions of the momentum equations:

$$\begin{aligned} 0 &= \delta v_R[\omega^2 - k^2 v_{Az}^2 - k_R^2(v_{A\phi}^2 + c_0^2) + ik_R k_z \frac{v_{Az}v_{A\phi}}{\omega}\frac{d\Omega}{d\ln R} + ik_R k_z c_0^2 \frac{D_1}{\omega}\sin\theta\cos\theta\frac{d\Omega}{d\ln R} \\ &- k_R^2 c_0^2 D_1] \;+\; \delta v_\phi\left[k_R k_z v_{Az} v_{A\phi} - 2i\Omega\omega + k_R k_z c_0^2 D_1 \sin\theta\cos\theta\right] \\ &- \delta v_z\left[k_R k_z(c_0^2 + v_{A\phi}^2) + k_R k_z c_0^2\cos^2\theta D_1\right], \end{aligned} \tag{23}$$

$$\begin{aligned} 0 &= \delta v_R[\frac{i\kappa^2\omega}{2\Omega} - i\frac{k_z^2 v_{Az}^2}{\omega}\frac{d\Omega}{d\ln R} + v_{A\phi}v_{Az}k_R k_z + k_z k_R c_0^2 D_1\sin\theta\cos\theta \\ &- i\frac{c_0^2 k_z^2}{\omega}(D_2 + D_1)\sin^2\theta\cos^2\theta\frac{d\Omega}{d\ln R}] + \delta v_\phi\left[\omega^2 - k_z^2 v_{Az}^2 - k_z^2 c_0^2\sin^2\theta\cos^2\theta(D_2 + D_1)\right] \\ &+ \delta v_z\left[k_z^2 v_{A\phi}v_{Az} - k_z^2 c_0^2 D_2\sin^3\theta\cos\theta + k_z^2 c_0^2 D_1\sin\theta\cos^3\theta\right] \end{aligned} \tag{24}$$

$$\begin{aligned} 0 &= \delta v_R[-k_R k_z(v_{A\phi}^2 + c_0^2) + ik_z^2\frac{v_{A\phi}v_{Az}}{\omega}\frac{d\Omega}{d\ln R} - k_z k_R c_0^2 D_1\cos^2\theta + i\frac{k_z^2 c_0^2}{\omega}D_1\cos^3\theta\sin\theta\frac{d\Omega}{d\ln R} \\ &- i\frac{k_z^2 c_0^2}{\omega}D_2\sin^3\theta\cos\theta\frac{d\Omega}{d\ln R}] + \delta v_\phi\left[k_z^2 v_{A\phi}v_{Az} - k_z^2 c_0^2 D_2\sin^3\theta\cos\theta + k_z^2 c_0^2 D_1\cos^3\theta\sin\theta\right] \\ &+ \delta v_z\left[\omega^2 - k_z^2(v_{A\phi}^2 + c_0^2) - k_z^2 c_0^2 D_2\sin^4\theta - k_z^2 c_0^2 D_1\cos^4\theta\right], \end{aligned} \tag{25}$$

where

$$v_{Az}^2 \equiv \frac{B_z^2}{4\pi\rho_0} \quad \text{and} \quad v_{A\phi}^2 \equiv \frac{B_\phi^2}{4\pi\rho_0} \tag{26}$$

are the Alfvén speeds associated with the vertical and azimuthal fields, respectively. Equations (23)-(25) define a matrix equation of the form $A\delta\mathbf{v} = 0$. Setting $\det(\mathrm{A}) = 0$ gives the dispersion relation. We have not found it particularly illuminating to write out the entire dispersion relation, nor have we made much progress solving it analytically, so instead we proceed to discuss its numerical solution. We will also present a simple model problem that captures the essential physics of the kinetic MRI.

The MHD dispersion relation for the MRI, including the effects of compressibility, can be obtained from equations (23)-(25) by setting $D_1 = D_2 = 0$. Equations (14) and (15) show that, for $D_1 = D_2 = 0$, $\delta p_\perp = \delta p_{||} = \delta\rho c_0^2$, i.e., the perturbations are isothermal and the perturbed pressure is isotropic. Our basic linear perturbation equations (eqs. [7]-[13]) reduce to their MHD analogues in this limit. In particular, note that in MHD the MRI is independent of whether the perturbations are adiabatic or isothermal; this is because it is an incompressible instability so the precise form of the sound speed is irrelevant for $\beta \gg 1$ (e.g., BH91). Thus the key simplification to the kinetic equations obtained by setting $D_1 = D_2 = 0$ is that the perturbed pressure becomes isotropic, as it is in MHD.

3. Linear Waves in Double Adiabatic Theory

Before considering the full kinetic MRI problem, it is instructive to consider the simpler problem of linear waves in a uniform medium. In particular, we show that the slow magnetosonic wave is very different in kinetic theory than in MHD. This is important for understanding the kinetic MRI because the slow wave, along with the Alfvén wave, is central to the dynamics of the MRI. We use double adiabatic theory throughout this section. Although double adiabatic theory does not include collisionless damping, which is quite strong for the slow mode and would alter some of the results in this section, it does show the significant differences introduced by the anisotropic pressure in a collisionless plasma. Since our interpretation of the kinetic MRI in §4 focuses on the importance of this anisotropic pressure, it is useful to see its implications first in a simpler problem. In §4 and the Appendix we show that the qualitative conclusions drawn in this section carry over to the full kinetic analysis.

Double adiabatic theory in a uniform medium corresponds to setting $\Omega = \kappa = 0$ and $\xi \gg 1$ in equations (23)-(25), in which case $D_1 = 1$ and $D_2 = 2$. Without loss of generality we can take $B_\phi = 0$ so that $\cos\theta = 0$ and $\sin\theta = 1$. To make contact with standard notation, we also write $k_r = k_\perp$, $k_z = k_\|$, and $v_{Az} = v_A$. The dispersion relation is then given by

$$\left[\omega^2 - k_\|^2 v_A^2\right]\left[(\omega^2 - k^2 v_A^2 - 2k_\perp^2 c_0^2)(\omega^2 - 3k_\|^2 c_0^2) - k_\perp^2 k_\|^2 c_0^4\right] \equiv D_A D_{MS} = 0. \tag{27}$$

The analogous MHD dispersion relation is

$$\left[\omega^2 - k_\|^2 v_A^2\right]\left[(\omega^2 - k^2 v_A^2 - k_\perp^2 v_s^2)(\omega^2 - k_\|^2 v_s^2) - k_\perp^2 k_\|^2 v_s^4\right] = 0, \tag{28}$$

where $v_s^2 = \gamma c_0^2$ is the adiabatic sound speed and $\gamma = 5/3$ is the adiabatic index.

Equation (27) shows that, as in MHD, the double adiabatic dispersion relation factors into two parts: an Alfvén wave branch ($D_A = 0$) and a magnetosonic branch ($D_{MS} = 0$). The Alfvén wave in double adiabatic theory is identical to that in MHD, while the magnetosonic waves are different – this is because the "adiabatic index" in a collisionless plasma is different for motions perpendicular and parallel to the magnetic field. Motion along the field is one-dimensional and corresponds to $\gamma = 3$ (hence the $3k_\|^2$ term in eq. [27]) while motion perpendicular to the field is two-dimensional and corresponds to $\gamma = 2$ (hence the $2k_\perp^2$ term in eq. [27]). By contrast, in MHD, the pressure is isotropic and $\gamma = 5/3$.

Figure 1 shows a plot of the dispersion relation of the fast and slow magnetosonic waves in MHD (dotted lines) and in double adiabatic theory (solid lines), taking $\beta = 100$. The fast wave, which is essentially a sound wave, is qualitatively similar in the two cases (the quantitative differences are due to the different γ's). The slow wave, however, is quite different. In MHD, the dispersion relation of the slow wave is degenerate with that of the Alfvén wave for $\beta \gg 1$, namely $\omega = k_\| v_A$. Except for $k_\perp = 0$, this is not true in double adiabatic theory. The frequency of the slow wave depends on the sound speed; in fact, for $k_\perp \neq 0$, the primary restoring force for the slow wave in double adiabatic theory is gas pressure, not magnetic forces.

This result can be understood as follows. In MHD, the properties of the $\beta \gg 1$ slow wave can be calculated by explicitly imposing incompressibility, $\nabla \cdot \delta\mathbf{v} \propto \delta\rho \approx 0$. This additional constraint (incompressibility) replaces the equation of state to determine the pressure (the Boussinesq approximation). In a collisionless plasma, this cannot happen because the pressure response is different parallel and perpendicular to the magnetic field, i.e., there are *two* equations of state (one for $p_\perp$ and one for $p_\|$). Both equations of state cannot be replaced by the single requirement that the fluctuations be incompressible. More physically, a $k_\perp \sim k_\|$ slow wave in MHD has $\delta p \sim \delta B^2/8\pi \sim B_0\ \delta B_\perp/4\pi$, i.e., the gas pressure, magnetic pressure, and magnetic tension forces are all comparable. Equivalently, $\delta p/p_0 \sim \beta^{-1}\delta B/B_0 \ll \delta B/B_0$ (for $\beta \gg 1$). In double adiabatic theory, however, a parallel magnetic field perturbation $\delta B/B_0$ induces a pressure perturbation $\delta p_{\perp,\|}/p_0$ of comparable magnitude (see eqs. [18] and [19]). This means that the pressure forces are much larger than the magnetic forces ($\delta p \sim \beta\ \delta B^2/8\pi \gg \delta B^2/8\pi$) and dominate the dynamics of the wave.

The exception to these arguments is if the pressure perturbation vanishes, i.e., $\delta p_\perp = \delta p_{||} = 0$. Alfveń waves and the $k_\perp \to 0$ limit of the slow magnetosonic wave are the only waves in MHD that have $\delta p = 0$ (they also have $\delta B = 0$). As a result, these pressure-free waves are the only incompressible fluctuations in double adiabatic theory. For all other waves, and in particular for slow waves with $k_\perp \neq 0$, pressure is the dominant restoring force in a $\beta \gg 1$ plasma and so the frequencies depend strongly on the sound speed (Fig. 1).

The results in this section are relevant to the MRI because the MRI is an incompressible instability with $|\omega| \ll kc_0$. Although pressure forces generally lead to a small modification of the MRI in MHD, they will be substantially more important in the kinetic analysis (just as for the slow magnetosonic wave in this section).

4. The Kinetic MRI

As noted in §2.3, the general kinetic MRI dispersion relation appears to be analytically intractable. In this section we present its numerical solution and physical interpretation. As a check on our numerical calculations we have confirmed that our results reproduce the kinetic dispersion relation for the Alfvén wave and the slow and fast magnetosonic waves when $\Omega = 0$ (including the collisionless damping rates).[6] We also reproduce the MRI in MHD when the kinetic terms are dropped (this requires setting $D_1 = D_2 = 0$ in eqs. [23]-[25]).

Figures 2-4 show the results of numerically solving the kinetic MRI dispersion relation, assuming a Keplerian disk for which $\Omega \propto R^{-3/2}$ and $\kappa = \Omega$. The figures show the kinetic growth rate of the MRI for different values of $\beta_z \equiv 8\pi p_0/B_z^2$, for different magnetic field geometries (defined by B_ϕ/B_z), and for different wavevectors (k_R and k_z). The corresponding MHD results are shown for comparison by the dotted lines. It is important to note that in MHD the MRI growth rate is essentially independent of β and B_ϕ/B_z; by contrast, Figures 2-4 show that the kinetic results depend sensitively on both of these parameters.

Figures 2-4 show that, although the growth rates can be very different, the region of instability in wavevector space is the same in kinetic theory and MHD. To understand this result, it is sufficient to consider the $\omega \to 0$ limit of the kinetic equations, since this determines the transition between stable and unstable modes. Setting $\omega = 0$ implies that $\xi \equiv \omega/(\sqrt{2}k_{||}c_0) = 0$ as well. From equations (14)-(16), it then follows that $\delta p_\perp/p_0 = \delta p_{||}/p_0 = \delta\rho/\rho_0$. Physically, as $\xi \to 0$, there is more and more time for particles moving

---

[6] We compared our results to the linear kinetic code described in Quataert (1998) and to the analytic results in Barnes (1966) and Foote & Kulsrud (1979).

along magnetic field lines to efficiently transport heat. This leads to nearly isothermal fluctuations in which the pressure perturbation is isotropic and is set only by the density perturbation. As discussed in §2.3, the kinetic equations reduce to the MHD equations in this limit. This is an important result because it shows that the MHD instability criterion, namely $d\Omega^2/dR < 0$, applies to the kinetic problem as well. Moreover, the set of unstable modes is the same in MHD and kinetic theory, as is seen explicitly in Figures 2-4.

Perhaps the three most striking results of the kinetic calculation shown in Figures 2-4 are: (1) The kinetic growth rates depend sensitively on β. For $\beta \gg 1$ they differ significantly from the MHD growth rates while for $\beta \sim 1$ they are similar (see Fig. 3). (2) For $B_\phi = 0$, or for sufficiently large k_R, the kinetic growth rates are smaller than their MHD counterparts, particularly at large β (e.g., Fig. 3a). (3) For $B_\phi \neq 0$, the kinetic growth rates can be *larger* than their MHD counterparts (e.g., Fig. 2 and Fig. 4b). Moreover, for $\beta \gg 1$, the fastest growing mode is at $k_z v_{Az} \ll \Omega$, where there is negligible growth in MHD (Fig. 4b).

To understand the kinetic MRI results, we have found it useful to consider the equations that describe the displacement of a fluid element from its equilibrium circular orbit. BH92 and BH98 showed that, for the special case of a vertical magnetic field and vertical wavevector, the radial and azimuthal components of the MHD momentum equation can be written in terms of the radial and azimuthal fluid displacements, ξ_R and ξ_ϕ, as

$$\frac{\partial^2 \xi_R}{\partial t^2} - 2\Omega \frac{\partial \xi_\phi}{\partial t} = -\left(\frac{d\Omega^2}{d\ln R} + (k_z v_{Az})^2\right)\xi_R, \tag{29}$$

$$\frac{\partial^2 \xi_\phi}{\partial t^2} + 2\Omega \frac{\partial \xi_R}{\partial t} = -(k_z v_{Az})^2 \xi_\phi. \tag{30}$$

As discussed by BH92 and BH98, equations (29) and (30) are identical to the equations describing two orbiting point masses connected by a spring of spring constant $k_z^2 v_{Az}^2$ (in MHD, magnetic tension plays the role of the spring). This suggests the following physical interpretation of the MRI in MHD (BH92). For a rotation profile with $d\Omega^2/dR < 0$ (unstable to the MRI), a fluid element at radius $R - \delta R$ is rotating slightly faster than a fluid element at radius R. The "spring" pulls backwards on this inner fluid element, removing its angular momentum and forcing it to move to a yet smaller radius. Similarly, a fluid element at radius $R + \delta R$ is rotating slightly slower than a fluid element at radius R and so the "spring" pulls forward on this fluid element, giving it angular momentum and forcing it to move to a yet larger radius. This simple physical picture captures the essence of the MRI in MHD.

A useful toy model that provides additional insight into the physics of the MRI, both in MHD and kinetic theory, is given by the following equations for the fluid displacement

$$\frac{\partial^2 \xi_R}{\partial t^2} - 2\Omega \frac{\partial \xi_\phi}{\partial t} = -\left(\frac{d\Omega^2}{d\ln R} + K_R\right)\xi_R, \tag{31}$$

$$\frac{\partial^2 \xi_\phi}{\partial t^2} + 2\Omega \frac{\partial \xi_R}{\partial t} = -K_\phi \xi_\phi. \tag{32}$$

Equations (31) and (32) describe the displacement of rotating fluid elements coupled by an anisotropic "spring," for which the spring constant is different in the azimuthal (K_ϕ) and radial (K_R) directions (this is clearly no longer a real spring!). The unstable root in the dispersion relation associated with equations (31) and (32) is given by

$$\omega^2 = \frac{\kappa^2 + K_R + K_\phi}{2} - \frac{1}{2}\left[\left(K_\phi + K_R + \kappa^2\right)^2 - 4K_\phi\left(K_R + \frac{d\Omega^2}{d\ln R}\right)\right]^{1/2}. \tag{33}$$

For $K_R = K_\phi = (k_z v_{Az})^2$, equation (33) gives the $k_R = 0$ dispersion relation of the MRI in MHD (this is shown by the dotted line in Fig. 4b). It is also straightforward to show that, for $K_R > K_\phi$, the growth rates in equation (33) are smaller than the MHD growth rates (i.e., those with $K_R = K_\phi$) and for $K_\phi > K_R$ the growth rates in equation (33) are larger than the MHD growth rates. For example, for $K_\phi = 0$, equation (33) gives $\omega = 0$ for any K_R and so there is no instability. On the other hand, the $K_\phi \gg \Omega \gg K_R$ solution of equation (33) is $|\omega| \approx \sqrt{|d\Omega^2/d\ln R|}$. For a Keplerian disk this gives $|\omega| = \sqrt{3}\Omega$, which is larger than the growth rate of the fastest growing mode in MHD ($|\omega| = 3\Omega/4$).

These results can be understood physically by noting that it is ultimately the presence of an azimuthal restoring force, rather than a radial restoring force, that is *destabilizing* in the MRI. This is because it is the azimuthal force that removes angular momentum from an inwardly displaced fluid element and adds it to an outwardly displaced fluid element. By contrast, the radial force is stabilizing because it attempts to "pin" the fluid element to its equilibrium position. Thus $K_\phi > K_R$ leads to faster growth because it enhances the destabilizing azimuthal force relative to the stabilizing radial force (and vice-versa for $K_R > K_\phi$). For the remainder of this section we explain how thermal pressure in a collisionless plasma plays the role of the anisotropic "spring" in the above toy model. This will account for the behavior of the kinetic MRI seen in Figures 2-4.

Because they are restricted to $k_R = 0$ and $B_\phi = 0$, equations (29) and (30) do not include the effects of gas pressure or magnetic pressure (both of which vanish in this special case). To understand the kinetic MRI we need to include these restoring forces using the radial and azimuthal momentum equations (eqs. [8] and [9], respectively). This yields the following equations for the fluid displacement[7]

$$\frac{\partial^2 \xi_R}{\partial t^2} - 2\Omega \frac{\partial \xi_\phi}{\partial t} = -\left(\frac{d\Omega^2}{d\ln R} + (k_z v_{Az})^2\right)\xi_R - ik_R\left(\frac{\delta B^2}{8\pi\rho_0} + \frac{\delta p_\perp}{\rho_0}\right), \tag{34}$$

$$\frac{\partial^2 \xi_\phi}{\partial t^2} + 2\Omega \frac{\partial \xi_R}{\partial t} = -(k_z v_{Az})^2 \xi_\phi - ik_z\left(\frac{\delta p_{||} - \delta p_\perp}{\rho_0}\right)\sin\theta\cos\theta. \tag{35}$$

In equations (34) and (35) we have simply rewritten the pressure gradients from equations (8) and (9); in the Appendix we calculate these explicitly in terms of the fluid displacement. It is worth noting again that there is a pressure force in the ϕ-momentum equation (eq. [35]) because the perturbed pressure is anisotropic. In MHD, $\delta p_{||} = \delta p_\perp$ and so this term vanishes.

Following the arguments in §3 and Figure 1 we expect that the pressure gradients in equations (34) and (35) will be much more important in kinetic theory than in MHD. In the Appendix we calculate the magnitude of these pressure forces and confirm this hypothesis. We use these results below to present a physical interpretation of the kinetic MRI, focusing on two important special cases: (1) $B_\phi = 0$, $k_R \neq 0$, for which the kinetic growth rates are smaller than their MHD counterparts (e.g., Figs. 3a & 4a), and (2) $k_R = 0$, $B_\phi \neq 0$, for which the kinetic growth rates are larger than the MHD growth rates (e.g., Fig. 4b).

Consider first the special case of $B_\phi = 0$ and $k_R \neq 0$ (e.g., Fig. 3a & 4a). In this case a displaced fluid element feels a restoring force in the radial direction due to gas and magnetic pressure; there is, however, no analogous pressure gradient in the ϕ direction (only magnetic tension). This corresponds to $K_R > K_\phi$ in the toy model of equation (33); the growth rates should therefore be suppressed with respect to the $k_R = 0$ growth rates. The presence of a stabilizing radial pressure gradient provides a physical explanation for why the MHD growth rates decrease with increasing k_R (see, e.g., the dotted line in Fig. 3a). Moreover, in the Appendix we show that the pressure gradient in kinetic theory is larger than in MHD by a factor of $\sim \beta^{1/2}$. The kinetic growth rates should therefore be even smaller than the MHD growth rates, with stronger suppression at larger β. This is precisely what is seen in the kinetic calculation; e.g., Figures 3a and 4a show the $B_\phi = 0$ growth rate for different β.

Consider now the special case of $k_R = 0$, but $B_\phi \neq 0$ (e.g., Fig. 4b). In this case the radial pressure force vanishes, but there is an azimuthal pressure force due to the anisotropic pressure. As suggested by the toy model in equation (33) this azimuthal pressure force, which is not present in MHD, is *destabilizing* because it removes angular momentum from

[7]Strictly speaking, equations (30) and (35) should have an additional term on the right hand side given by $k_z v_{Az} v_{A\phi}(\mathbf{k}\cdot\xi)$. For $\beta \gg 1$, this term is negligible because the MRI is nearly incompressible and so we do not consider it further.

an inwardly displaced fluid element and adds it to an outwardly displaced fluid element (just as the azimuthal component of magnetic tension does). Moreover, for $B_\phi \sim B_z$ the destabilizing pressure force is larger than the destabilizing magnetic tension force by a factor of $\sim \beta^{1/2}$ (see the Appendix). This explains why the $k_R = 0$, $B_\phi \neq 0$ growth rates are larger than their MHD counterparts, and why the growth rates increase with increasing β (see, e.g., Fig. 4b). It also explains why the growth can be rapid even at $k_z v_{Az} \ll \Omega$, when magnetic tension (which drives the MRI in MHD) is very weak. In fact, for $\beta \gg 1$ and $k_z v_{Az} \ll \Omega$, the forces in the kinetic MRI are arranged as follows: azimuthal pressure $\gg$ Coriolis $\gg$ magnetic tension. We therefore expect the growth rates to approach the $K_\phi \gg \Omega \gg K_R$ limit of equation (33), namely $|\omega| \approx \sqrt{3}\Omega$. As shown in Figure 4b, the fastest growing modes do approach this maximal growth rate.

Although the above interpretation focuses on two special cases, the results in Figures 2-4 can be readily understood as a competition between the stabilizing radial pressure force and the destabilizing azimuthal pressure force. The importance of gas pressure, rather than magnetic forces, also explains why the kinetic results depend sensitively on β.

5. Summary and Discussion

In this paper we have presented a linear axisymmetric calculation of the magnetorotational instability (MRI) in a collisionless plasma. Our analysis is restricted to wavelengths much larger than the proton Larmor radius, frequencies below the proton cyclotron frequency, and "seed" magnetic fields with no radial component ($B_R = 0$). The MRI is believed to give rise to MHD turbulence and efficient angular momentum transport in astrophysical accretion flows, and may also be important for the dynamo generation of galactic and stellar magnetic fields (e.g., BH98). Our kinetic calculation, rather than an MHD calculation, is appropriate whenever the collisional mean free path of the protons exceeds the wavelength of the MRI.

The instability criterion for the kinetic MRI is the same as in MHD, namely that the angular velocity decrease outwards. The set of unstable modes is also the same in kinetic theory and MHD. However, nearly every mode has a linear kinetic growth rate that differs from its MHD counterpart. For example, the fastest growing mode in kinetic theory has a growth rate $\approx \sqrt{3}\Omega$ for a Keplerian disk, which is larger than its MHD counterpart by a factor of $4\sqrt{3}/3 \approx 2.3$.[8] More generally, the kinetic growth rates can be either larger or smaller than the MHD growth rates, depending on the orientation of the magnetic field and the wavevector of the mode (Fig. 2). The kinetic growth rates also depend explicitly on β,

[8]This rapid growth is obtained only for $k_R v_{Az} \ll \Omega$, $k_z v_{Az} \ll \Omega$, $\beta \gg 1$, and $B_\phi \gtrsim B_z$ (see Figs. 3 & 4).

i.e., on the ratio of the gas pressure to the magnetic pressure. For $\beta \gg 1$ the kinetic results differ significantly from the MHD results while for $\beta \sim 1$ they are similar (see Fig. 3).

We have argued that the kinetic MRI can be understood by considering the force due to pressure gradients in a high β collisionless plasma. In MHD, pressure leads to a relatively minor modification of the MRI. In kinetic theory, however, the pressure forces are $\sim \beta^{1/2}$ times larger than in MHD and are therefore dynamically much more important (see §3 and the Appendix). Moreover, in kinetic theory there is an azimuthal pressure force even for axisymmetric modes (so long as $B_\phi \neq 0$; see eqs. [10] and [35]). This is because the pressure response is anisotropic in a collisionless plasma: it is different along and perpendicular to the local magnetic field. This azimuthal pressure force, which is not present in MHD, is *destabilizing* because it removes angular momentum from an inwardly displaced fluid element and adds it to an outwardly displaced fluid element (just as the azimuthal component of magnetic tension does in MHD). The destabilizing pressure force explains why the kinetic growth rates of the MRI can be larger than the MHD growth rates (e.g., Fig. 4b).

The importance of gas pressure shows that the character of the MRI is somewhat different in a collisionless plasma than in a collisional plasma described by MHD. The crucial function of the magnetic field is to enforce an anisotropic pressure response, rather than to directly destabilize the plasma via magnetic tension. The importance of pressure gradients also explains why the kinetic results depend sensitively on β. For $\beta \sim 1$ pressure forces are comparable to magnetic forces, and the kinetic growth rates are not that different from the MHD growth rates, while for $\beta \gg 1$ pressure forces dominate over magnetic forces and the kinetic results differ substantially from the MHD results (e.g., Fig. 3).

BH92 showed that the MRI in MHD could be understood using a simple model in which magnetic tension acts like a spring coupling different fluid elements in the plasma. We have presented a generalization of BH92's "spring" model that captures many of the results of the full kinetic MRI calculation (see eqs. [31]-[33]). In this model the radial and azimuthal "spring constants" are different; physically, this corresponds to the anisotropic pressure response in a collisionless plasma.

To conclude, we briefly discuss the astrophysical implications of our results, focusing on the two applications mentioned in the introduction: (1) the amplification of weak fields generated by a Biermann battery or analogous mechanism, and (2) hot two-temperature accretion flows onto compact objects.

(1) For a very weak magnetic field MHD predicts that the fastest growing mode of the MRI has a very small wavelength $\approx v_A/\Omega \propto B$. This will be less than the collisional mean free path in many cases. Our kinetic analysis shows that there is rapid growth of the MRI

even in this limit. This is encouraging for the hypothesis that the MRI contributes to the dynamo amplification of very weak magnetic fields, e.g. the generation of galactic fields from a cosmological seed field. To further assess this question, however, it is necessary to extend our analysis to include finite Larmor radius effects. In particular, the "battery" generation of magnetic fields is limited by self-induction to field strengths such that the proton Larmor radius is comparable to the size of the system (e.g., Balbus 1993). Finite Larmor radius effects will always be important on these scales, particularly since the wavelengths of unstable MRI modes are then much less than the proton Larmor radius.

(2) In radiatively inefficient accretion flows onto compact objects, which have been applied extensively to low-luminosity accreting sources (e.g., Narayan et al. 1998), the inflowing gas is a hot two-temperature plasma in which the proton temperature is much larger than the electron temperature. In order to maintain $T_p \gg T_e$, the timescale for electrons and protons to exchange energy by Coulomb collisions must be longer than the inflow time of the gas. This requires a sufficiently small accretion rate, $\dot{M} \lesssim \dot{M}_{crit} \approx \alpha^2 \dot{M}_{EDD}$ (e.g., Rees et al. 1982), where $\dot{M}_{EDD}$ is the Eddington accretion rate and α is the dimensionless Shakura-Sunyaev viscosity parameter. Since the timescale for proton-electron collisions to modify the proton distribution function is comparable to the proton-electron energy exchange timescale, the proton dynamics is effectively collisionless for *all* radiatively inefficient accretion flows;[9] the kinetic calculation presented in this paper is therefore appropriate for describing angular momentum transport by the MRI in such models.[10]

It is, however, difficult to apply our linear calculations to the nonlinear saturated state expected in the accretion flow. Nonetheless it is worth noting that there are rapidly growing modes in a collisionless plasma even for $\beta \gg 1$ so weak fields can be efficiently amplified. Moreover, MHD simulations find saturation at $\beta \sim 1 - 100$ with a predominantly toroidal field (e.g., BH98; Stone & Pringle 2001). For this magnetic field configuration, the linear kinetic growth rates of the MRI are not that different from their MHD counterparts (if anything, they may be somewhat larger; e.g., Figs. 3b & 4b). While this suggests that the saturated turbulence may be qualitatively similar in kinetic theory and MHD, there will undoubtedly be quantitative differences. In addition, the fact that the fastest growing modes occur at somewhat different wavenumbers could change the nonlinear results. Perhaps more importantly, collisionless damping of the sound wave and the slow magnetosonic wave is very strong and operates on all scales in a collisionless plasma, while strong damping in MHD is

[9]Electron-proton collisions are more important than proton-proton collisions because $T_p \gg T_e$.

[10]By contrast, geometrically thin accretion disks (e.g., Shakura & Sunyaev 1973) are much cooler and denser; MHD accurately describes the dynamics of thin disks so long as the gas is sufficiently ionized.

restricted to very small scales. This may alter the nonlinear behavior of the MRI. Numerical simulations that address these issues would be extremely interesting.

Our results may also have implications for understanding particle heating in radiatively inefficient accretion flows. The radiative efficiency of such models is set by the amount of electron heating in the plasma. This depends on how the energy in MHD turbulence is dissipated (e.g., via a turbulent cascade, reconnection, etc.). The prominent role of pressure fluctuations in the kinetic MRI suggests that the resulting turbulence may couple better to slow waves (which have a pressure perturbation) than Alfvén waves (which do not). Slow waves primarily heat the protons in the collisionless plasmas of interest (e.g., Quataert 1998; Blackman 1999) while an Alfvènic cascade may lead to significant electron heating if $\beta \lesssim 10$ (e.g., Gruzinov 1998; Quataert & Gruzinov 1999). Kinetic simulations of the MRI should be able to assess the relative importance of slow wave and Alfvén wave excitation.

We thank Steve Balbus, Steve Cowley, Barrett Rogers, Alex Schekochihin, and Anatoly Spitkovsky for useful discussions. GH was supported in part by the U.S. Department of Energy under Contract DE-AC02-76CH03073. EQ was supported in part by NASA grant NAG5-12043.

REFERENCES

Armitage, P. J., 1998, ApJ, 501, L189

Balbus, S. A., 1993, ApJ, 413, L137

Balbus, S. A. & Hawley, J. F., 1991, ApJ, 376, 214 (BH91)

Balbus, S. A. & Hawley, J. F., 1992, ApJ, 392, 662 (BH92)

Balbus, S. A., & Hawley J. F., 1998, Rev. Mod. Phys., 70, 1 (BH98)

Barnes, A. 1966, Phys. Fluids, 9, 1483

Blackman, E., 1999, MNRAS, 302, 723

Chew, G. F., Goldberger, M. L., & Low, F. E., 1956, Proc. R. Soc. London, Ser. A, 236, 112

Foote, E. A. & Kulsrud, R. M. 1979, ApJ, 233, 302

Gruzinov, A., 1998, ApJ, 498, 458

Hawley, J. F., 2000, ApJ, 528, 462

Hawley, J. F., Gammie, C. F., & Balbus, S. A., 1995, ApJ, 440, 742

Kulsrud, R. M., 1983, in *Handbook of Plasma Physics*, ed. M. N. Rosenbluth and R. Z. Sagdeev (North Holland, New York)

Ichimaru, S. 1977, ApJ, 214, 840

Narayan, R., & Yi, I. 1995, ApJ, 452, 710

Narayan, R., Mahadevan, R., & Quataert, E. 1998, in *Theory of Black Hole Accretion Discs*, ed. M. Abramowicz, G. Bjornsson, & J. Pringle (Cambridge: Cambridge Univ. Press)

Shakura, N.I. & Sunyaev, R.A. 1973, A&A, 24, 337

Quataert, E., 1998, ApJ, 500, 978

Quataert, E. & Gruzinov, A., 1999, ApJ, 520, 248

Quataert, E. 2001, in *Probing the Physics of AGN with Multiwavelength Monitoring*, ed. B. M. Peterson, R. S. Polidan, & R. W. Pogge (San Francisco: Astr. Soc. Pacific), p. 71

Rees, M. J., Phinney, E. S., Begelman, M. C. & Blandford, R. D., 1982, Nature, 295, 17

Snyder, P. B., Hammett, G. W., & Dorland, W., 1997, Phys. Plasmas, 4, 11

Stix, T.H. 1992, *Waves in Plasmas* (New York: AIP)

Stone, J. & Pringle, J., 2001, MNRAS, 322, 461

A. Calculation of the Pressure Forces

In this Appendix we calculate the radial and azimuthal pressure forces in equations (34) and (35) in terms of the fluid displacements ξ_R and ξ_ϕ. These are used in our interpretation of the kinetic MRI results in §4. We restrict our analysis to the two important limits highlighted in §4: (1) $B_\phi = 0; k_R \neq 0$ and (2) $B_\phi \neq 0; k_R = 0$.

A.1. $B_\phi = 0; k_R \neq 0$

In this case there is a radial pressure force given by (eq. [34])

$$F_R \equiv -ik_R \left(\frac{\delta B^2}{8\pi\rho_0} + \frac{\delta p_\perp}{\rho_0}\right) = -ik_R \left[\frac{\delta\rho}{\rho_0}c_0^2 + \frac{\delta B}{B_0}\left(v_{Az}^2 + D_1 c_0^2\right)\right], \tag{A1}$$

where we have used $\delta p_\perp / p_0 = \delta\rho/\rho_0 + D_1 \delta B/B_0$ from equation (14) in the second equality. We now rewrite all of the terms in F_R in terms of ξ_R, the radial displacement. For $B_\phi = 0$, $\delta B = \delta B_z$. The radial component of the induction equation (eq. [11]) thus yields

$$\frac{\delta B}{B_0} = \frac{k_R \delta v_R}{\omega} = -ik_R\xi_R. \tag{A2}$$

To calculate $\delta\rho/\rho_0 = (k_z\delta v_z + k_R\delta v_R)/\omega$ in terms of ξ_R alone we need to find δv_z as a function of δv_R. To do this note that the z-component of the momentum equation (eq. [10]) implies

$$k_z \delta v_z = \frac{k_z^2 \delta p_{||}}{\omega\rho_0}. \tag{A3}$$

Since $\delta\rho/\rho_0 - \delta B/B_0 = k_z\delta v_z/\omega$, equation (15) gives $\delta p_{||}$ as a function of both δv_z and δv_R. Substituting this into equation (A3) we solve for δv_z in terms of δv_R and thus find

$$\frac{\delta\rho}{\rho_0} = -ik_R\xi_R\left(1 + \frac{c_0^2 k_z^2}{\omega^2 - c_0^2 k_z^2 (1 + D_2)}\right). \tag{A4}$$

Substituting equations (A2) and (A4) into equation (A1), and assuming $\beta \gg 1$ so that $|\omega^2| \ll k_z^2 c_0^2$, yields

$$F_R = -k_R^2\xi_R\left[c_0^2\left(D_1 + \frac{2D_2}{1+2D_2}\right) + v_{Az}^2\left(1 - \frac{\omega^2}{k_z^2 v_{Az}^2 (1+2D_2)^2}\right)\right]. \tag{A5}$$

The MHD limit of equation (A5) can be obtained by setting $D_1 = D_2 = 0$ (see §2.3). In this case $F_R = -\xi_R k_R^2 v_{Az}^2 [1 + |\omega|^2/(k_z^2 v_{Az}^2)] \sim -\xi_R k_R^2 v_{Az}^2$. Consider instead double adiabatic theory, for which $D_1 = 1$ and $D_2 = 2$. In this case $F_R \sim -\xi_R k_R^2 c_0^2$; this is larger than the MHD pressure force by a factor of $\sim \beta$. Finally, for the full kinetic problem we need to evaluate D_1 and D_2 using equation (16). Since the MRI has $|\omega| \lesssim k_z v_A$ we can take $\xi \ll 1$ so long as $\beta \gg 1$. In this case $D_1 \approx D_2 \approx -i\sqrt{\pi}\xi \sim -i\omega/k_z c_0$, so that $F_R \sim -k_R^2 \xi_R c_0^2(-i\omega/k_z c_0)$. To estimate the magnitude of F_R, note that $|\omega| \sim k_z v_A$ in MHD, in which case $F_R \sim -\xi_R k_R^2 v_{Az} c_0$. This is $\sim \beta^{1/2}$ times larger than the pressure force in MHD. This large radial pressure gradient suppresses the growth rates of the MRI, as seen in Figures 2-4.

A.2. $B_\phi \neq 0; k_R = 0$

In this case there is an azimuthal pressure force given by (eq. [35])

$$F_\phi \equiv -ik_z \sin\theta\cos\theta \frac{\delta p_\| - \delta p_\perp}{\rho_0} = -ik_z c_0^2 \sin\theta\cos\theta \left[D_2 \frac{\delta\rho}{\rho_0} - (D_1 + D_2)\frac{\delta B}{B_0}\right], \qquad \text{(A6)}$$

where we have used equations (14) and (15) to eliminate $\delta p_\perp$ and $\delta p_\|$. For $\beta \gg 1$ the MRI is nearly incompressible and $\delta\rho/\rho_0 \ll \delta B/B_0$.[11] We therefore neglect the $\delta\rho/\rho_0$ term in equation (A6). Using $\delta v_\phi = \partial\xi_\phi/\partial t - \xi_R d\Omega/d\ln R$ one can rewrite equation (22) for δB in terms of ξ_ϕ. Again neglecting $\delta\rho/\rho_0$ relative to the other terms, this yields

$$\frac{\delta B}{B_0} = -ik_z \sin\theta\cos\theta\xi_\phi. \qquad \text{(A7)}$$

Substituting equation (A7) into equation (A6) yields

$$F_\phi = -\xi_\phi k_z^2 c_0^2 \sin^2\theta\cos^2\theta(D_2 + D_1). \qquad \text{(A8)}$$

In MHD, $F_\phi = 0$, and magnetic tension, which $\sim -k_z^2 v_{Az}^2 \xi_\phi$ (see eq. [35]), plays the destabilizing role. By contrast, in kinetic theory the azimuthal pressure force is given by $F_\phi \sim -\xi_\phi \sin^2\theta\cos^2\theta k_z^2 c_0^2(-i\omega/k_z c_0)$. For $B_\phi \sim B_z$, so that $\sin\theta \sim \cos\theta \sim 1$, this is larger than the destabilizing azimuthal tension force by a factor of $\sim \beta^{1/2}$. This large destabilizing azimuthal pressure force enhances the growth rates of the MRI, as seen in Figures 2-4.

[11]The calculation in Appendix A.1 shows this explicitly: eqs. [A4] and [A2] imply that $\delta\rho/\rho_0 \sim D_2\delta B/B_0$ where $D_2 \sim \beta^{-1/2} \ll 1$. The same qualitative result holds for the different geometry considered here.

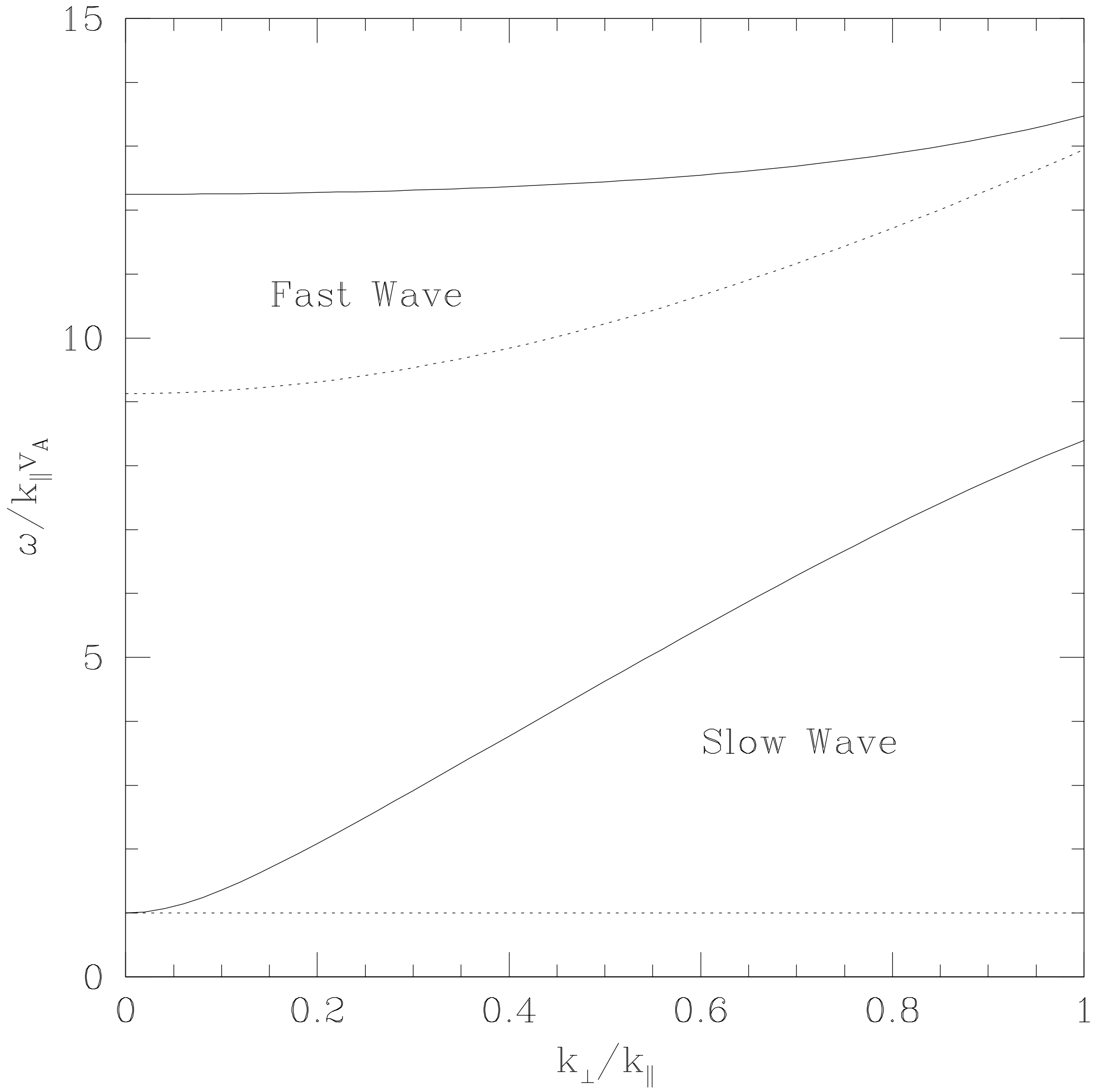

Fig. 1.— The dispersion relation for the magnetosonic waves in MHD (dotted lines) and in double adiabatic theory (solid lines), taking $\beta = 100$. In MHD, the slow wave dispersion relation is identical to that of the Alfvén wave ($\omega = k_\| v_A$) while this is only true for $k_\perp \ll k_\|$ in double adiabatic theory (see the text for an explanation).

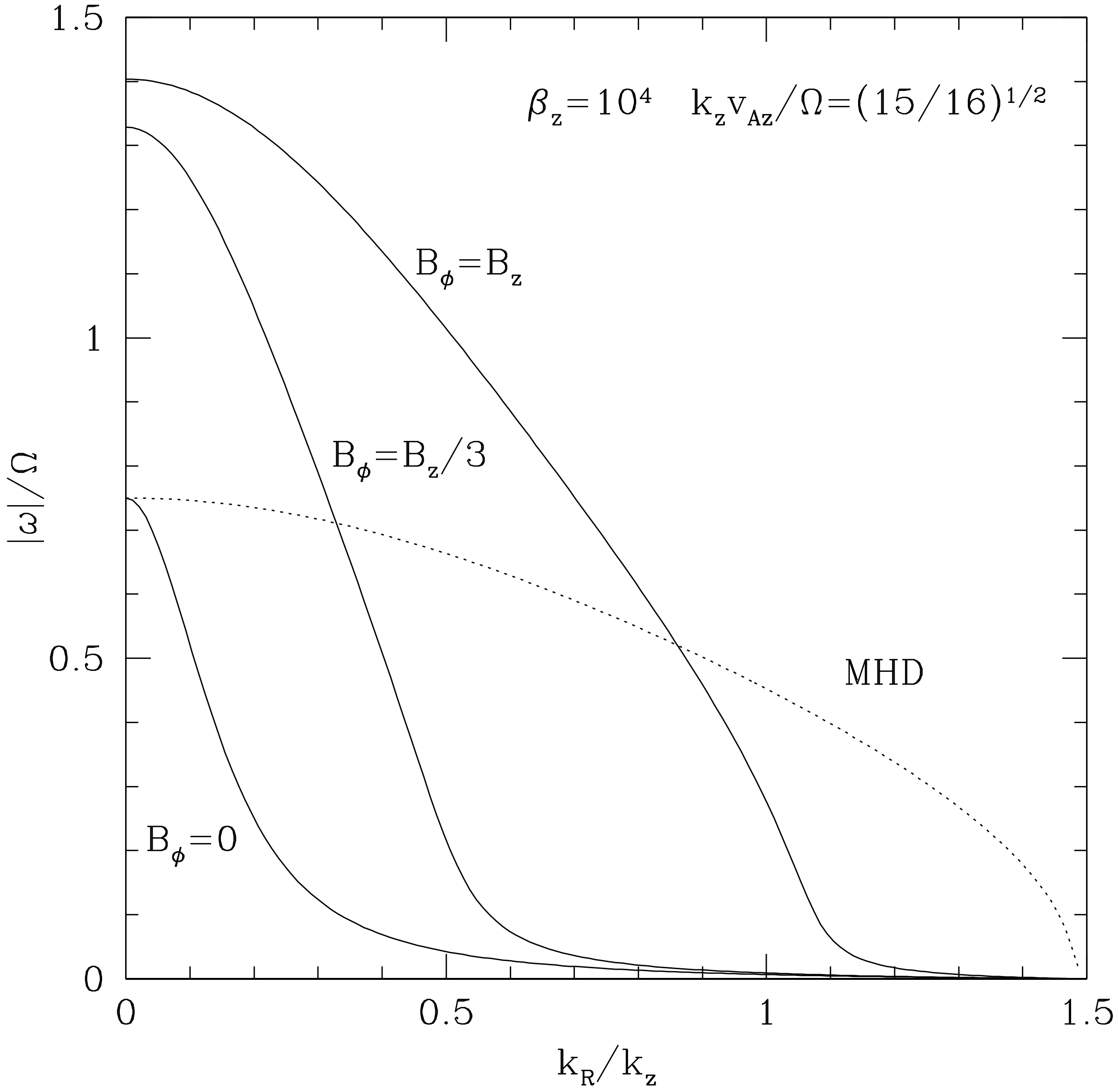

Fig. 2.— The kinetic growth rates of the MRI for $\beta_z \equiv 8\pi p_0/B_z^2 = 10^4$ and for different geometries of the seed magnetic field. The MHD results, which are independent of B_ϕ, are shown for comparison (dotted line). The vertical wavenumber is taken to be $k_z v_{Az}/\Omega = \sqrt{15/16}$, which is the fast growing mode in MHD.

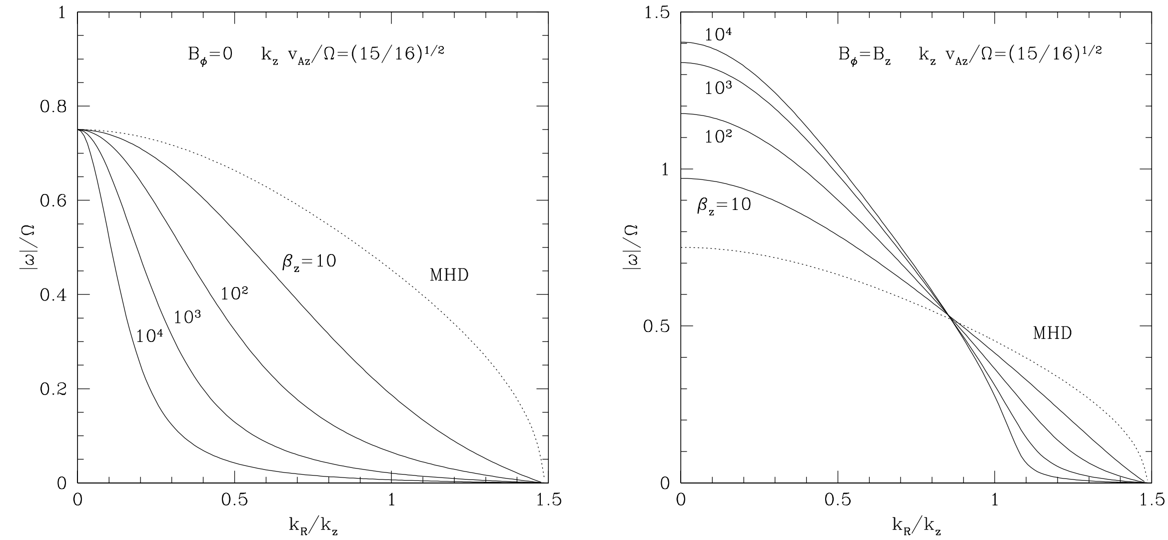

Fig. 3.— The kinetic growth rates of the MRI for varying β_z (solid lines). The MHD results, which are nearly independent of β_z, are shown for comparison (dotted line). The vertical wavenumber is taken to be $k_z v_{Az}/\Omega = \sqrt{15/16}$, which is the fast growing mode in MHD.

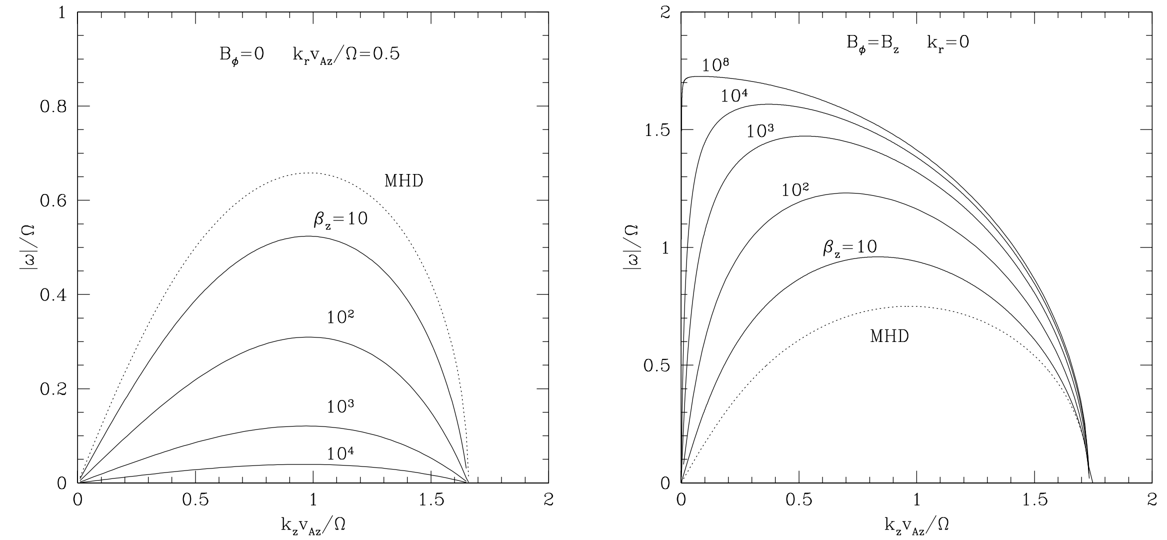

Fig. 4.— The kinetic growth rates of the MRI as a function of k_z for different β_z (solid lines). The corresponding MHD results are shown by the dotted line.